Proceedings of ASME Turbo Expo 2003
Power for Land, Sea, and Air
June 16–19, 2003, Atlanta, Georgia, USA

GT2003-38853

Side Air-Jet Modulation for Control of Heat Release and Pattern Factor

Onur Tuncer[†]**,**
Department of Mechanical Engineering,
Louisiana State University, Baton Rouge, LA, 70803
otunce1@lsu.edu

Sumanta Acharya[‡]
Department of Mechanical Engineering,
Louisiana State University, Baton Rouge, LA, 70803
acharya@me.lsu.edu

Jeff Cohen[#]
United Technologies Research Center,
East Hartford CT 0618

Andrzej Banaszuk[#]
United Technologies Research Center
East Hartford CT 0618

ABSTRACT

The effect of a forced dilution air jet introduced through the combustor shell, on the air-fuel mixing in the combustion chamber has been investigated. Thermocouple based temperature measurements have been made at a number of forcing frequencies in the range of 100-1100Hz and blowing ratios in the range of 10-15. The open-loop integral flame response to forcing has also been acquired by recording pressure and heat release spectra. A CH-radical imaging technique is used to provide spatially- and temporally- resolved information about the heat release behavior. The results exhibit that the mean temperature field inside the main reaction zone can significantly be altered as a consequence of air jet modulation. The most significant effects are observed by forcing at vertical locations that are close to the dump plane. Enhancements in temperature of the order of 100–200 degrees C, and reduction in pattern factor of the order of 10% (e.g., from 1.13 to 1.03) were observed, with the lowest pattern factors achieved at the lowest forcing frequency of 100 Hz.

Keywords: spray combustion, mixing, forced dilution jet

NOMENCLATURE

C Holdeman parameter $C = \left(S/D/2\right)\sqrt{J}$

D Combustor diameter
F/A Fuel to air ratio
H Combustor height
J Jet to main flow momentum flux ratio
L Length scale
M Mach number $M = \frac{U}{c}$
PF Pattern Factor $PF = \frac{T_{\max} - T_o}{\overline{T} - T_o}$
R Blowing ratio R= u_{jet}/U_∞
S Circumferential spacing between orifice centers $S = \pi\left(D/\sqrt{2}\right)/n$
Re Reynolds number $\mathrm{Re} = uL_c/\nu$
St Strouhal number $St = \frac{fL_c}{U}$
T Temperature
a Distance between two parallel jet axis
c Speed of sound $c = \sqrt{\gamma RT}$
d Jet exit diameter

[†] Graduate Student
[‡] L.R Daniel Professor, Corresponding Author

[#] Research Engineer
[#] Research Engineer

f Frequency
$\dot{m}$ Mass flow rate
n Number of jet injection holes
r Radial position
u Velocity
z Elevation measured from the dump plane

Greek Symbols

γ Specific heat ratio
λ Wavelength
ν Kinematic viscosity
ρ Density
θ Azimuthal position
ϕ Equivalence ratio $\phi = \frac{\left(F/A\right)_{actual}}{\left(F/A\right)_{stochiometric}}$

Subscripts

c Characteristic
max Maximum
o Inlet
jet Dilution jet
∞ Main flow
¼ Quarter wave mode
¾ Three quarter wave mode
* Excited state

Superscripts

¯ Average

INTRODUCTION

Key performance metrics for gas turbine combustors and propulsion systems include volumetric heat release, pattern factor and emissions. These metrics are controlled primarily by the combustor stochoimetry, and the degree of fuel-air mixing. In a typical non-premixed combustor, both fuel and combustion air are introduced longitudinally at the dump plane, and swirl is generally utilized to mix the fuel and air streams together. In certain combustor designs, additional primary and dilution air are introduced radially through circumferential holes located along the combustor shell. These air-jets in cross flow not only provide the air needed to control the stochiometry, but also generate enhanced fuel-air mixing. Therefore the proper design and utilization of these air-jets can provide a means toward controlling the fuel-air mixing, and enhancing the performance metrics. Increased mixedness, for example, can provide lower pattern factor, lower emissions, and higher volumetric heat release.

Numerous experimental and numerical studies have been carried out on the structure of turbulent transverse jets, and have shown that, the entrainment and mixing processes can be enhanced by modulating the jet flow [1-9]. These studies suggest that the enhanced entrainment is mainly due to the structural formation of counter rotating vortex pairs [5], and/or due to toroidal vortices, which are formed close to the jet exit [1]. For high blowing ratios, wake vortices behind the jet are also observed [6]. Acoustic forcing is found to trigger certain modes of these vortex instabilities that have Lagrangian dynamics [5]. There is a general agreement in the literature that the open-loop jet response is optimized at the preferred mode jet frequencies that correspond to Strouhal numbers in the range of $0.1<St<0.3$ [1, 4, 6, 9]. The enhanced vortex dynamics and entrainment of the cross-flow leads to increased molecular mixing between the air and fuel species that, in turn, control the combustion processes and the heat release. Since the heat release influences the temperature, the measured temperature distribution inside the combustion chamber can be used to quantify the enhanced entrainment and mixing processes in the combustor.

Vermuelen et. al. [2] attempted to modify the exit plane temperature distribution of a combustor by acoustically modulating the dilution air-jet-streams located close to the exit plane. A difference in temperature of the order of 10^0C was observed with modulation due to increased jet mixedness. Further, the uniformity in the temperature distributions appeared to be influenced favorably by the modulation.

The goal of the present experimental study is to manipulate fuel-air mixing in a swirl-stabilized spray combustor through modulation of the side-air jets, and to examine the impact of this manipulation on the pattern factor and volumetric heat release. It is expected that modulation of the air-jets will provide improved fuel-air mixing, and that the greatest impact will be achieved at a specific frequency. As pointed out by Holdeman et al. [10,11], the goal of an improved design should not only be to reduce the PF to its lowest value, but to achieve this over the shortest possible distance. As noted earlier, greater uniformity in the temperature distribution or lower pattern factor is important for a variety of reasons: (1) thermal gradients and stresses acting on the turbine blades can be reduced thereby extending blade life, (2) NOx emissions are likely to be reduced by eliminating hot spots, and (3) volumetric heat release in the main reaction zone is enhanced by increasing the temperatures in the cold-spot regions near the end walls, and between the injectors. Furthermore, improved fuel-air mixing at a shortest possible height enables the design of compact propulsion systems.

EXPERIMENTAL APPARATUS

A schematic of the experimental setup showing all the major components is presented in Fig. 1. The combustor shell is cylindrical with a diameter (D) of 193.7 mm and a height (H) of 762mm. Ethanol (C_2H_5OH) fuel is injected at the center through a Parker-Hannifin Research Simplex Atomizing (RSA) nozzle, which has an approximate spray cone angle of 26º. A 45º-swirl vane with a 5 mm exit diameter through which atomization air is delivered surrounds the nozzle tip. Main combustion air is fed through a 45º-swirl vane with inner and outer diameters of 34 and 63 mm respectively (Fig. 2). The step height at the dump plane is nearly 65 mm. A 38 x 64 mm quartz window mounted on the shell enables optical access for CH imaging and photodiode measurements. A number of thermocouple ports are located at different elevations and angular locations, and type B thermocouples are used to map the temperature distribution inside the combustor. Typically, a rake with four thermocouples mounted on an automated traverse is used for obtaining the temperature distributions inside the combustor.

Fuel is delivered to the combustor through a tank pressurized by compressed nitrogen. A dual gage pressure regulator controls the upstream pressure of the nitrogen gas to

achieve the desired fuel flow rate. The air needed for the atomization, for primary combustion and the side air-jets are all delivered through independent compressed air lines each controlled by individual pressure regulators and needle valves. The compressed air lines feed off large storage tanks fed by a 290psig, 450ACFM Atlas-Copco air compressor.

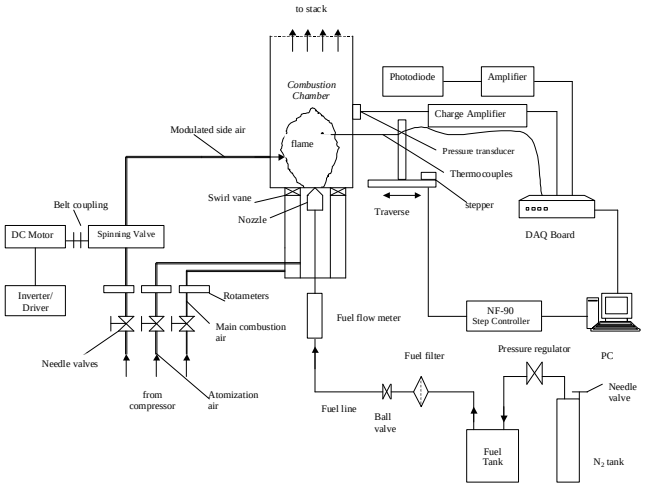

Figure 1. Schematic Layout of the Experimental Setup

Injection holes for side-air jets each 9.5 mm diameter and uniformly distributed in the circumferential direction are located at several elevations along the combustor height (Fig. 2). In this study, four injection holes (n=4) located at an elevation z/D of 0.2 and circumferential spacing S/D of 0.56 (where S is defined as per Holdeman [10]) are chosen in order to modulate the main reaction zone. The circumferential location of the four injection holes are shown in Fig. 3, and are chosen such that they have a certain offset (a/D = 0.16) with respect to each other. This offset magnitude was chosen arbitrarily, and no optimization of this offset has been attempted in this paper. The offset direction is such that the injected air assists the swirling motion of the main combustion air, and can provide varying degrees of swirl depending on the momentum ratio of the injected air.

The modulation of the side-air is accomplished by routing it via a spinning valve which has a hollow disk with 20 holes drilled at its periphery rotating inside a stationary housing that has two discharge holes [12]. As the spinner element rotates, the stationary and moving holes match at a frequency governed by the rotational speed of the spinner element. A representative time history of jet exit velocity measured by a hotwire anemometer is shown in Fig. 4. The air jet velocity varies around a mean value at a frequency dictated by the rotational speed of the spinner element. The velocity output is not a pure sinusoid due to the non-negligible contributions from the harmonic components, which arise from the non-linearities in the system. The strength of the velocity modulations is proportional to the airflow rate and the frequency of the spinning valve. The frequency response of the spinning valve in the range of 50- 1000 Hz (range of interest to the present study) is shown in Fig. 5, and does not show a perfectly flat response. Rather, the response is somewhat uneven due to the acoustic eigenfrequencies of the spinning valve with variations in the

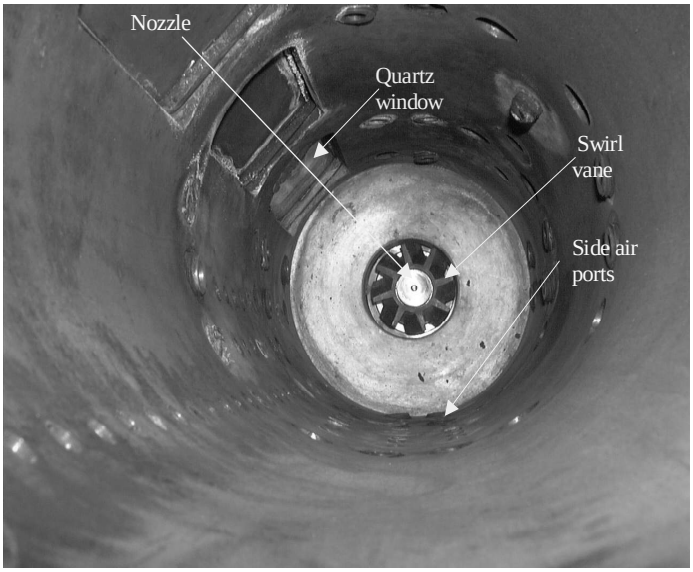

Figure 2. Inside View of the Combustion Chamber

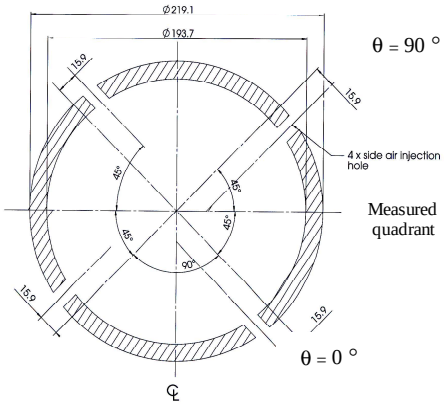

Figure 3. Section View of the Combustor at z/D= 0.2 Depicting the Side Air Injection Holes (All dimensions in mm.)

range of 74dBau-86dBau. At higher frequencies, the response drops off, and if the frequency response were to be plotted over a broad range of frequencies, it would show a relatively flat region (variations of the order shown in Fig. 5) at lower frequencies followed by a rapid decay at higher frequencies. Since it was anticipated that the side-air jet would be most responsive for modulation in the Strouhal number range of 0.1-0.4, only the lower frequency range (St<0.4, f<1.5 kHz) is of interest to the present study, and the frequency response is examined only in this region. Since both forcing frequency and forcing amplitude are important parameters, frequencies are chosen based on where the response is high (Fig. 5), and such that the amplitude of modulation at these frequencies is nearly the same (to allow for a comparative assessment of the role of modulation or forcing frequency). The selected frequencies are 100, 300, 450, 600, 850 and 1100 Hz, and as seen in Fig. 6, the maximum amplitude variation in this range is about 4dBau.

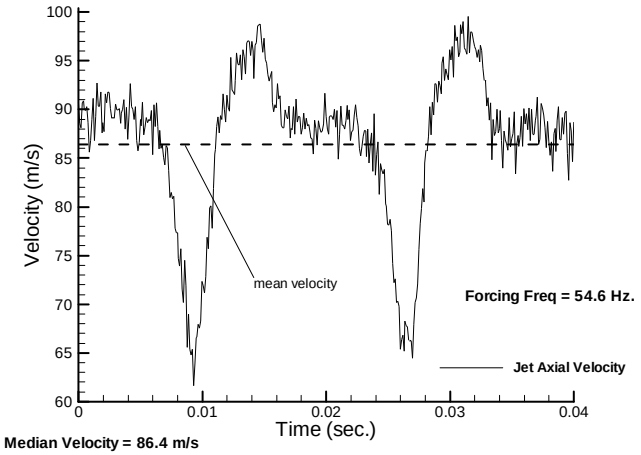

Figure 4. Time History of Jet Exit Velocity

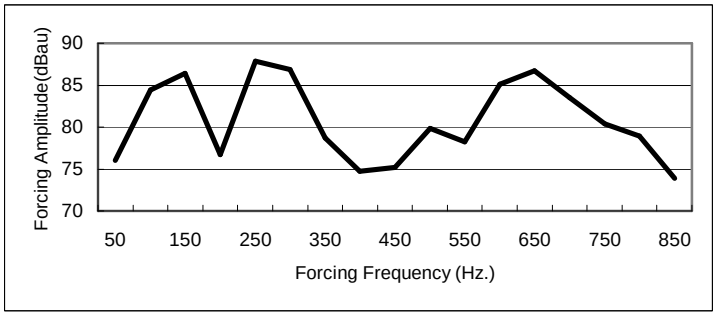

Figure 5. Frequency Response of the Spinning Valve

The fuel and airflow rates are obtained by a series of rotameters and pressure gauges. The measurement accuracy of the air and fuel flow rates are ± 2.0 % and the measurement accuracy for the pressure gauges mounted at the exit of air flow meters are ± 1.0 %. This yields an overall measurement accuracy of ± 4.5 % in the equivalence ratio.

Temperature is measured by Type B Pt-Ro thermocouples. Each set of temperature data is obtained using a thermocouple rake that is inserted inside the reacting flow and than traversed radially outwards with a VELMEX-1500 series X-Z traverse controlled by a NF-90 Stepper-Motor Controller and a personal computer. Temperature readings are averaged over a time period of 30 seconds with 2000 samples collected at each point to ensure that no averaging errors are introduced. Thermocouple readings are corrected for radiation losses. Overall repeatability of the temperature measurements is determined to be ± 20 K.

The pressure variations in the combustor and the heat release from the flame are also measured. The integral heat release is arbitrarily quantified with a photodiode looking at the flame. An optical CH filter mounted on the photodiode allows the light at λ=390 nm, corresponding to the CH radical emission, to pass through and attenuates all other wavelength contributions. A Kistler 7061 water-cooled piezo-electric pressure transducer is mounted along the combustor walls, and measures the pressure inside the combustion chamber. Both the heat release and pressure spectra are computed with an SRS-785 spectrum analyzer. An intensified CCD camera is used to resolve the temporal and spatial heat release characteristic through cycle resolved CH imaging technique.

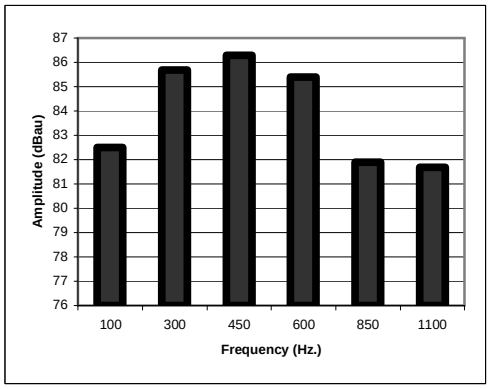

Figure 6. Relative Forcing Amplitude with respect to Forcing Frequency

RESULTS AND DISCUSSION

The combustor is operated close to stochiometric conditions with an overall equivalence ratio (based on total air through the front end and the side jets) of ϕ = 0.9. NOx emissions are particularly high at near stochiometric conditions [13], and reduction in pattern factor is likely to help in reducing NOx. While the impact of side air-jet modulation on the pattern factor will be explored in the present study, measurements of NOx have not been undertaken. These measurements are planned for a later phase of the research.

The data is taken at two distinct blowing ratios R= u_{jet}/U_∞ of 15 and 10. The front-end equivalence ratios (based on air delivered only through the front-end) are ϕ =1.7 and ϕ =1.4 for R=15 and R=10 respectively. The equivalence ratio is held constant during modulation of the side air-jets. As noted earlier, the side air-jet is modulated at six different frequencies (100 Hz, 300 Hz, 450 Hz, 600 Hz, 850 Hz, 1100 Hz.) with comparable excitation amplitudes (see Fig. 6) in order to allow an unbiased comparison of the effect of the modulation frequencies without influencing this effect by the forcing amplitude. The Strouhal numbers ($St = \frac{fd}{u_{jet}}$, where f is the forcing frequency and d is the jet exit diameter) corresponding to the six forcing frequencies are: St=0.026, 0.078, 0.118, 0.157, 0.222, 0.288 at a blowing ratio of 15, and St=0.034, 0.102, 0.152, 0.203, 0.288, 0.372 at a blowing ratio of 10.

The flow rates corresponding to an overall equivalence ratio of 0.9: fuel flow rate of 0.03 l/s atomization airflow rate of 0.5 l/s, and primary combustion air and the side air-jet flow rates of 11.8 l/s and 10.3 l/s respectively for the blowing ratio of 15, and 14.2 l/s and 8.0 l/s respectively for the blowing ratio of 10. At these flow rates, the jet Reynolds number Re_{jet} ($\mathrm{Re}_{jet} = u_{jet} L / \nu$, where $L = \left(\dot{m}_{jet} u_{jet} / \rho U_\infty^{\,2} \right)^{1/2}$ as suggested by Broadwell et. al. [14]) is 2.9×10^5 for R=15, and is 1.5×10^5 for

R=10. The corresponding cross flow Reynolds numbers $\mathrm{Re}_\infty = U_\infty D / \nu$ for these the cases are 3×10^3 and 3.5×10^3 for R=15 and R=10 respectively.

To establish a baseline to the degree of mixedness of the unforced jets with the mainstream Holdeman [10] used an empirical self-similarity parameter that he denoted as C. He recommended values of about 2.5 to be optimal. In the present study, the C values are considerably higher (19 and 12 for R=15 and 10 respectively). However, Holdeman's study is based on non-reacting, non-swirling flows in a cylindrical tube. The present flow field is considerably more complex, and therefore the optimal parameters recommended by Holdeman do not necessarily apply here. In particular, higher blowing and momentum flux ratios were necessary in the present study (compared to those recommended by Holdeman), and these contribute to the higher C values.

Temperature Profiles

Due to the very low Mach number of the main flow the temperatures measured by the thermocouples can essentially be interpreted as stagnation temperatures. The temperature data is presented only in the range $0.3 \le z/D \le 1.1$ where the jet-air mixing primarily takes place. However, it should be noted that combustion continues to take place further downstream, and at the exit of the combustor (z/D=4), the stack temperatures for the modulated and unmodulated cases are expected to be the same.

Figures 7a and 7b show temperature contours at different elevations for blowing ratios of 15 and 10 respectively. The contours are shown only for one quadrant between two side air-jets. Note that the side air-jets are introduced at z/D=0.2, and the axial locations shown in Fig. 7 are all downstream of the side air-jet injection. At z/D=0.3 (the elevation closest to the side air-jet injection), the signature of the unheated side air-jet introduced into the heated stream is clearly visible (low temperature region). The flame is partly quenched along the jet trajectory due to the high strain rates and since the local equivalence ratio ϕ falls below the lean extinction limit of 0.5 [15]. In the unforced case (St = 0) the jet can be said to be mostly concentrated around the periphery of the flame where a large cold region is evidently seen. Therefore, the jet-penetration, and the mixing around the jet periphery is quite poor. However, as the external forcing is introduced the distance that the jet penetrates along its axis towards the flame is significantly increased. Significantly enhanced jet penetrations are observed at St= 0.118 and 0.222 for R=15. Note that the two St values where the strongest penetration is observed are related to each other by a factor of 2, and potentially St=0.118 is close to a sub-harmonic of St=0.222. The strong jet penetration at St of 0.222 is in close agreement with the data of Vermeulen et. al. [1] where they report a St of 0.250 as an optimal value for jet penetration.

As the jet at R=15 is seen to penetrate deep into the flame regions at Strouhal numbers between 0.118 and 0.288, higher temperatures are observed downstream for these cases, compared to all other cases studied (St=0, 0.026,0.078). This is linked directly to the mixing enhancement and higher volumetric heat release induced by the jet modulation. While local enhancements in temperatures as large as 300^0C can be observed, the average enhancements appear to be more in the range of $50\text{-}100^0$C.

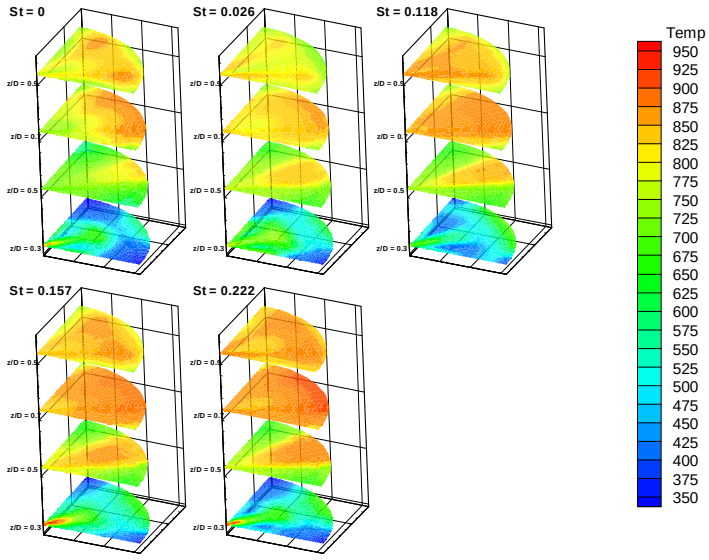

Figure 7. 3-D Temperature Contours at R=15 (Temperatures in°C)

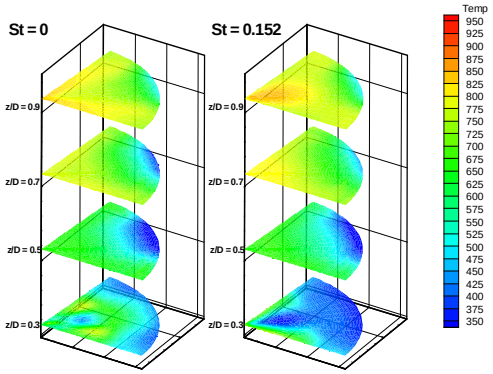

Figure 8. 3-D Temperature Contours at R=10 (Temperatures in°C

In comparing the baseline unmodulated case (St=0), with the modulated cases, it is clear that the uniformity in the temperature distribution is enhanced both radially as well as circumferentially with forcing. At z/D=0.7, for example, the baseline case shows significant radial variations in temperature with a cool inner core and a hot outer region where most of the burning takes place. With modulation and the associated enhanced mixing of the vaporized fuel and air, the radial distributions are relatively uniform. Thus, the forcing frequency not only influences the magnitude but also the uniformity. However, the range of frequencies where the maximum heat release occurs (St=0.118-0.222) does not correspond to the St value (0.026) with the most uniform distributions. More discussion on this issue is provided later in the section on Pattern Factors.

At a blowing ratio of 10 (Fig. 8), the effect of forcing is considerably reduced. This is associated with reduced jet penetration, and a smaller spatial region of influence. At St=0.152, the beneficial effects of modulation (higher

temperature and volumetric heat release) is more apparent at further downstream locations of z/D=0.7 and 0.9.

Figure 9 shows the radial distributions of temperature at different axial locations and one circumferential location ($\theta=36^0$) corresponding to the side-jet injection location. Note that the radial temperature distribution at a fixed azimuthal location is only representative of a local effect. For R=15, at z/D=0.56, 0.81, and 1.08, higher temperatures are obtained with forcing with differences of the order of 60-70 ^{0}C. Highest temperatures are generally obtained for St=0.222, while at St=0.118 (sub-harmonic) the temperature levels are comparably high but the distributions appear flatter. The flattest temperature distributions appear to correspond to the lowest modulation frequencies (St=0.026). At z/D=0.30, just downstream of the side air-jet injection location, the temperature distributions reflect the combined effects of localized flame quenching and enhanced mixing. For St numbers where the jet penetration is significant, the quenching effect is more apparent as in St=0.118. At the lowest frequency of St=0.026, jet penetration is not as large, but the effect of the increased mixing is significant and provides the flattest temperature distribution. As noted above, the flattest temperature distributions at downstream locations also correspond to the lowest modulation frequency (St=0.026).

For R=10, the general observations are consistent with those observed at R=15, except for differences in the levels of enhancement, and the relative roles of enhanced mixing vs localized quenching. At z/D=0.81 and 1.08, modulation increases the temperatures at St=0.102 and 0.152 due to the enhanced mixing effect, but at other modulation frequencies, this effect is not as strong, and temperatures even lower than the baseline can be seen due to localized quenching. The flattest temperature distributions are again achieved at the lowest Strouhal number considered for this blowing ratio.

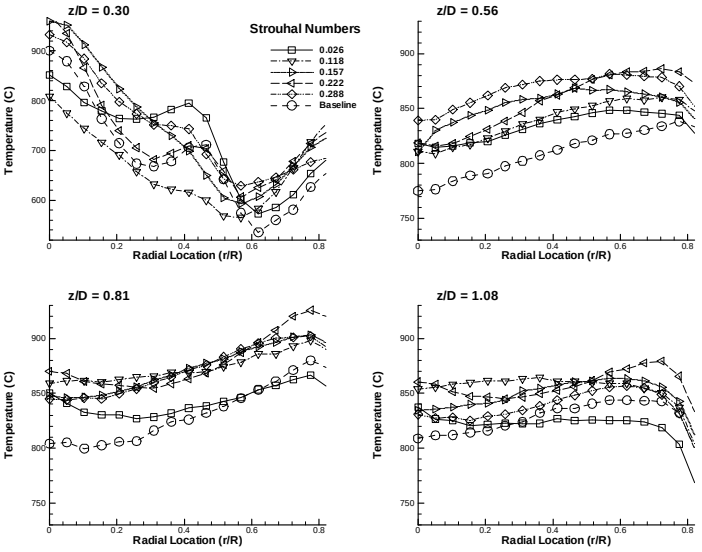

a. R=15, θ = 36°

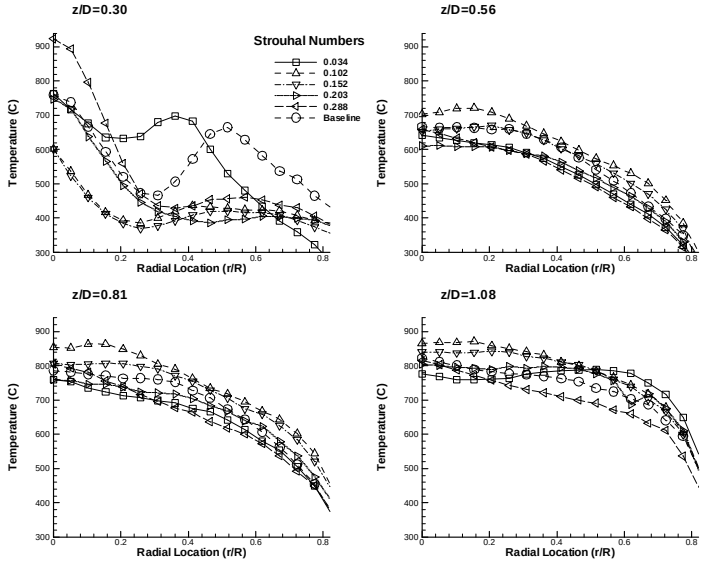

b. R=10, θ = 36°

Figure 9. Radial Temperature Profiles

Pattern Factors

The uniformity of the temperature profiles can be quantified by defining a pattern factor. A planar pattern factor (PF) is defined as follows in the present study:

$$PF(z) = \frac{T_{\max}(z) - T_o}{\overline{T}(z) - T_o} \tag{1}$$

where the radially weighted average temperature $\overline{T}(z)$ is the representative of the mean temperature in a (r,θ) plane. This is computed from the finite sum representation of the following equation,

$$\overline{T}(z) = \frac{\iint T(r,\theta,z) r dr d\theta}{\iint r dr d\theta} \tag{2}$$

Note that the pattern factors are dimensionless numbers and can attain a minimum value of 1.0 in the limiting case where there is no spatial variation in the temperature data. Low pattern factor values indicate a more uniform distribution with less variance in the temperature profile, whereas larger values signify stronger radial and circumferential thermal gradients.

Figure 10 shows the planar pattern factors plotted versus non-dimensional height (z/D) from the dump plane for the baseline case and at different forcing frequencies. Regardless of the modulation frequency, pattern factors decrease with increasing elevation due to increased mixing. However, practical perspectives limit the length of combustors, and are associated with unmixedness, but the goal of a combustion designer is to the design of compact combustors with low PF in a minimum combustor length.

It is helpful to interpret Fig. 10 with a perspective of the observations made in Figs. 8 and 9, which show the detailed temperature distributions inside the combustor. The most significant variation of the PF with different forcing frequencies occurs at elevations close to the dump plane. Further downstream (z/D>0.7), the PF plots become gradually closer. In the primary combustion region (z/D < 0.7), the differences between the pattern factors can range from 0.1 to 0.4 at both blowing ratios. This is a significant effect, and is clear evidence of the fact that the uniformity of the temperature field can be significantly altered with flow modulation, and that

the modulation frequency can play an important role. Nonetheless, these plots also do indicate a trade-off between the performance merits, that is, the frequency showing the most favorable heat release characteristics does not posses the minimum pattern factor.

At R=15, in general, modulation produces a decrease in PF over most of the combustor length, although over a short span (for z/D less than 0.4), there are frequencies showing higher pattern factor than the baseline condition. The lowest forcing frequency (St=0.026) clearly shows the lowest PF with a 0.25 reduction (nearly 16%) in PF close to the dump plane and decreasing to about a 0.07 (6%) relative to the unforced case reduction in PF at around z/D=0.7.

For R=10, PF results are not favorable, and show an increase over the baseline case at nearly all frequencies. Thus, while temperatures are enhanced with modulation (Fig. 9), the jet penetration and mixing are not strong enough to lead to a reduction in the PF. Rather, the localized quenching effect contributes to increasing the PF. Therefore, in order to utilize the side air-jets to reduce PF, they should have sufficient momentum and control-authority in order to enhance the mixing process.

Pressure and Heat Release Spectra

The combustion chamber is acoustically closed at one end and acoustically open at the other one. Therefore, the dominant acoustic mode of the combustion chamber corresponds to a ¼ wave mode [16]. This is seen in the Fourier spectra of pressure and heat release signals (see figure 11) where there is a peak at the quarter wave mode ($f_{1/4} = c/4H$) around 190 Hz. The other mode excited in the unforced case corresponds to a ¾ wave mode (λ=4/3H). But, the amplitude of this excitation is rather weak and can be neglected. The Strouhal number corresponding to the acoustic mode and the mainstream velocity ($St_\infty = f_{1/4} 4H / U_\infty = \frac{1}{M_\infty}$) is nearly 217, and is much higher than the Strouhal numbers associated with the side jet preferred mode. Therefore, in the present configuration there is no interaction between the side air-jet frequencies and the acoustic frequencies, and the observed effects are primarily hydrodynamical.

In figure 11, the spectral response of the pressure transducer and CH-photodiode are shown as a function of frequency. The CH-photodiode is centered on the quartz window at a distance of 265 mm, and has a complete view of the main reaction zone including the region where the side air-jets are injected. The spectra clearly show both the acoustic mode of the main combustor as well as the forcing frequency. The open loop forcing of the side air is seen not to alter the dominant mode of combustion. The added mode due to open loop forcing at a constant frequency is responsible for the alteration of the temperature field. At most frequencies, the amplitude of this mode is comparable to the amplitude of the dominant mode at the higher blowing ratio (R=15). At the lower blowing ratio (R=10) however, this amplitude is about 15-20 dB less then the amplitude of the dominant mode due to the lack of modulation strength delivered by the spinning valve. Therefore, at the lower blowing ratio, the control authority is not strong, and as noted earlier in the temperature contours (Fig. 8), and PF plots (Fig. 10) the beneficial effects at this lower blowing ratio are not as evident. Consequently, the amplitude of modulation plays a very important role in terms of establishing control authority over the flame.

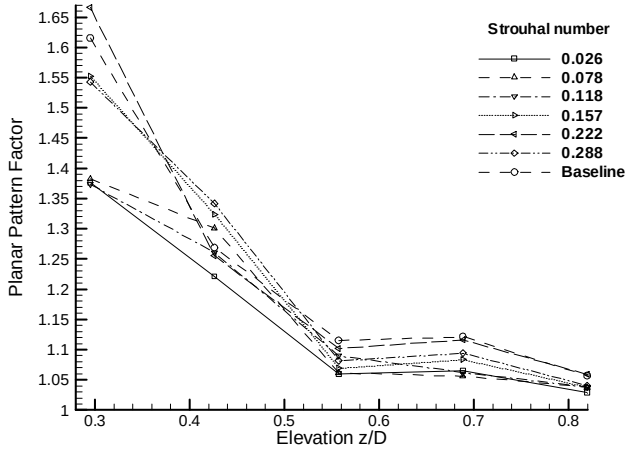

a. R=15

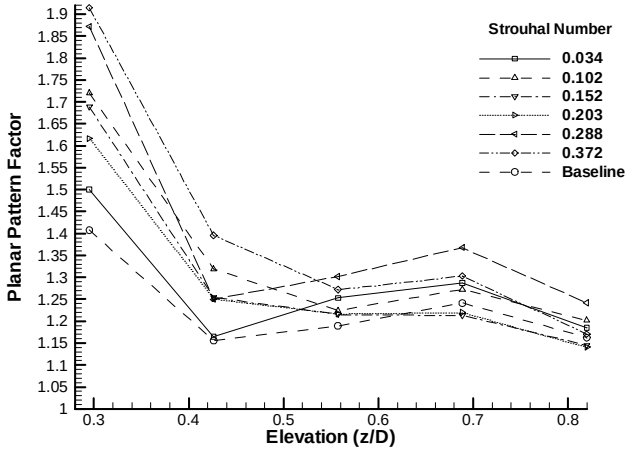

b. R=10

Figure 10. Planar Pattern Factors

The flame does not respond to pressure fluctuations roughly above 1.2 kHz. This is seen in figure 10, where for the 850 Hz forcing case, a strong second harmonic at 1.6 kHz in the pressure spectrum does not excite the corresponding heat release mode. Therefore, the response of the flame tapers-off above a finite frequency.

Chemiluminescence Measurements

In order to spatially resolve the temporal heat release characteristics in the reaction zone, chemiluminescence measurements of the CH radical were performed. The CH radicals have been shown to be representative of the ethanol flame front [17] and CH intensity correlates well with the local heat release for this type of fuel. An intensified Princeton Instruments PI-Max 512 T-18 G/III CCD camera with a

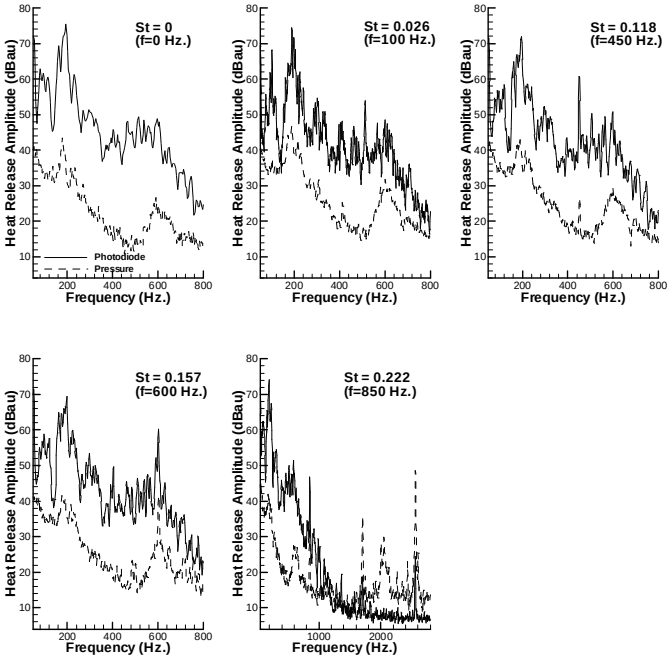

Figure 11. Pressure and Heat Release Spectra at R=15

512x512 pixel resolution was utilized to acquire the images. The gate duration for the image acquisition was set to 0.10 μs. A filter mounted on the camera lens is used to transmit the light at λ=390 nm which corresponds to the $B^2\Sigma^- - X^2\Pi(0,0)$ emission band of the CH radical [18], and to attenuate all other wavelength contributions. A KISTLER 7061B piezoelectric pressure transducer mounted at the downstream end of the spinning valve provided the phase information. The signal from the pressure transducer is fed into a DSPACE data acquisition board and the trigger signal (a TTL pulse) is generated at the selected phase angle to trigger the camera. To resolve the complete cycle at each phase angle a known time delay is added to the pressure signal. For the unmodulated case (St=0) the phase locking is performed with respect to the dominant mode of combustion. At each triggering condition a sequence of 50 images were recorded. These sequences are then averaged to yield the corresponding mean intensity field.

The CH images presented in this section are taken at both of the blowing ratios of 15 and 10. Figure 12 shows the phase averaged CH images at Strouhal numbers of 0 (steady side air-jet) and 0.026 at 90°-phase increments. The intensity images are presented on a pseudo-color scale with blue regions representing low CH-intensities, and red regions indicating high CH-levels. In the images the signatures of the side air jets are clearly seen on both the left side and the right side. The conical flame is stretched towards the side air jets indicating their impact on the flame combustion. At both St=0 and 0.026, the flame exhibits significant dynamics, with the dynamics at St=0.026 representing intrinsic heat release variations associated with either the acoustics or the unsteady hydrodynamics and mixing. Since the reference trigger at St=0 and St=0.026 are different, the respective images in Figs 12a and 12b cannot be directly compared, but it is evident that with modulation, the heat release variations are altered both spatially and temporally.

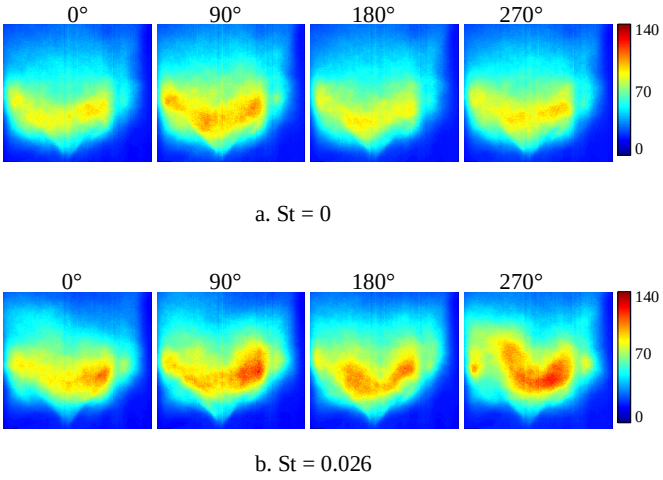

Figure 12. Phase Averaged CH Intensity Images at R=15

Figure 13 shows the time averaged CH-intensity distribution for the unmodulated (St=0) and modulated (St=0.026) cases at R=15, while Fig. 14 shows the corresponding standard deviation of the CH-intensity. It is obvious from Fig. 13 that with modulation (St=0.026) the time-averaged value of volumetric heat release within the reaction zone is enhanced by a significant amount. This is consistent with the 3-D temperature contour plots shown in Fig. 7. However, Fig. 14 suggest that the temporal fluctuations in the heat release are stronger with forcing This effect is due to larger velocity fluctuations associated with the side air jets.

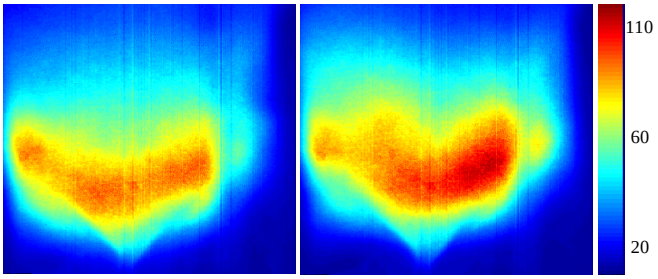

Figure 13. Time Averaged CH Intensity Images at R=15

CONCLUDING REMARKS

An experimental study is performed to explore the potential of modulating side air-jets in a non-premixed swirl-stabilized spray-combustor to enhance volumetric heat release (leading to more compact combustors) and to lower Pattern Factor (leading to lower emissions and reduced combustor length). It is shown that by modulating the side air-jets, the uniformity of the temperature profiles and the magnitude and distributions of the

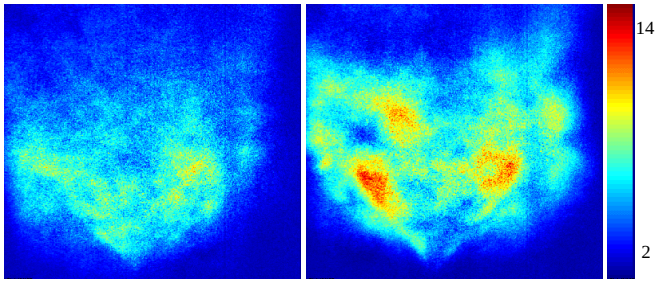

a. St = 0 b. St = 0.026

Figure 14. Pixelwise Standard Deviation at R=15

heat release patterns can be beneficially impacted. However, the two performance merits (volumetric heat release and Pattern Factor) do not show the same dependence on the modulation frequency. The highest enhancements in volumetric heat release occur at frequencies close to the fundamental and sub-harmonic modes of the side air jets (St of approximately 0.22 and 0.11 respectively for R=15). These modes are associated with the greatest jet penetration. The lowest Pattern Factor was seen to be observed at the lowest modulation frequency (St=0.026 for R=15) with reductions in PF ranging from nearly 16% close to the dump plane to about 6% for z/D>0.7. At a lower blowing ratio (R=10), the beneficial impacts of modulation were only observed in the volumetric heat release at select frequencies, and indicated the importance of the air-jet momentum as an important control parameter. For a significant effect the forcing must impose pressure fluctuations that are at least as strong as the ones coming from the dominant acoustic modes of combustion.

The success in the results obtained so far with open-loop control via side air-jet modulation points to the potential of a closed-loop control strategy for optimizing Pattern Factors, volumetric heat release, and emissions. The behavior of the plant at a multitude of load conditions can be construed as a dynamic neural network (DNN) for system identification purposes, and genetic algorithms can be utilized to determine the optimum-forcing conditions. Such closed-loop strategies will be explored in the future.

ACKNOWLEDGMENTS

The research was supported by the Propulsion Program of the Office of Naval Research under the guidance of Dr. Gabriel Roy. Their support is gratefully acknowledged. Helpful discussions with Dr. Satish Narayanan from UTRC, and Dr. Jeff Lovett from Pratt & Whitney are also acknowledged. Support to UTRC was provided by AFOSR grants F49620-98-C-0006 and F49620-01-C-0021.

REFERENCES

1. Vermeulen, P. J., Yu, W. K., 1985, “An Experimental Study of Mixing by an Acoustically Pulsed Axisymmettrical Air Jet”, ASME Paper No. 85-GT-49

2. Vermeulen, P. J., Odgers, Ramesh, V., 1982, “Acoustic Control of Dilution-Air Mixing in a Gas Turbine Combustor”, ASME Paper No. 82-GT-35

3. Johari, H., Pacheco-Tougas, M. and Hermanson, J. C., 1999, “ Penetration and Mixing of Fully Modulated Turbulent Jets in Crossflow”, AIAA Journal, **37**(7)

4. Blossey, P. N., Narayanan, S., Bewley, T. R., 2001,“Dynamics & Control of Jets in Crossflow Direct Numerical Simulations & Experiments”, Proceedings of IUTAM Symposium on Turbulent Mixing and Combustion

5. Cortolezzi, L., Karagozian, A. R., 2001, “On the Formation of Counter-Rotating Vortex Pair in Traverse Jets”, J. Fluid. Mech, **446**, pp.347-446

6. Narayanan, S., Barooah, P. and Cohen, J. M., 2002, “ Experimental Study of the Coherent Structure Dynamics & Control of an Isolated Jet in Cross Flow”, 40th Aerospace Sciences Meeting and Exhibit, Reno, Nevada

7. Cho, S. K., Yoo, J. Y., Choi, H., 1998, “Vortex Pairing in an Axisymmetric Jet Using Two-Frequency Acoustic Forcing at Low to Moderate Strouhal Numbers”, Experiments in Fluids, **25**, pp. 305-315

8. Karagozian et. al., 2002, “The Actively Controlled Jet in Crossflow”, J. Fluid Mech., **452**, pp. 325-335

9. Vermeulen, P. J., Ramesh, V., Yu, W. K., 1986, “ Measurements of Entrainment by Acoustically Pulsed Axisymmetric Air Jets”, Journal of Engineering for Gas Turbines and Power, **108**, pp. 479-484

10. Holdeman J.D., 1993, “Mixing of Multiple Jets with a Confined Subsonic Crossflow”, Prog. Energy Combust. Sci.,**19**, pp. 31-70

11. Holdeman J.D., Liscinsky D. S., Samuelson G. S., Oechsle, V. L., Smith, C. E., 1996, “Mixing of Multiple Jets with a Confined Subsonic Crossflow in a Cylindrical Duct”, ASME Paper No. 96-GT-482

12. O’Donnell, M., 2001, ”Spray Combustion Laser Diagnostics and Combustion control Via Air Flow Fluctuations”, Louisiana State University, Baton Rouge, LA

13. Roy, G., 1998, “Propulsion Combustion: Fuels to Emissions”, Taylor & Francis, Bristol

14. Broadwell, J. E., Breidenthal, R. E., “ Structure and Mixing of a Traverse Jet in Incompressible Flow”, Journal of Fluid Mechanics, Vol. 148, pp. 405-412

15. Westbrook, C. K., and Dryer, F. L., 1984, “Chemical Kinetic Modeling of Hydrocarbon Combustion”, Prog. Energy Combustion Sci., **10**, pp. 1-57

16. Culick, F. E. C., 1976, “Non-linear Behavior of Acoustic Waves in Combustion Chambers”, Acta Astronautica, **3**, pp.715-734

17. Bertran, C. A., Marques, C. S. T., Benvenutti, L.H., 1998, “Mapping of Luminescent Species in a Flame Front”, Combustion Science and Technology, **139**, pp. 1-13

18. Garland, N. L., Crosley, D.R., 1985, “Energy Transfer Processes in CH $A^2\Delta$ and $B^2\Sigma^-$ in an Atmospheric Pressure Flame”, Applied Optics, **24**, pp. 4229-4237

